Redox Hopping in Metal-Organic Frameworks through the Lens of the Scholz Model

Minliang Yan,[a] *Eric M. Johnson,*[b] *and Amanda J. Morris** [a,b]

a. Macromolecule Innovation Institute, Virginia Tech, Blacksburg, VA 24061, USA

b. Department of Chemistry, Virginia Tech, Blacksburg, VA, 24061, USA

Abstract

Initially proposed by Lovric and Scholz to explain redox reactions in solid-phase voltammetry, the Scholz model's applications have expanded to redox in various materials. As an extension of the Cottrell equation, the Scholz model enabled the quantification of electron hopping and ion diffusion with coefficients, D_e and D_i, respectively. Research utilizing the Scholz model indicated that, in most cases, a huge bottleneck is resulted from the ion diffusion which is slower than electron hopping by orders of magnitude. Therefore, electron and ion motion can be tuned and optimized to increase the charge transport and conductivity through systematic investigations guided by the

Scholz model. The strategy may be extended to other solid-state materials in the future, e.g., battery anodes/cathodes. In this perspective, the applications of the Scholz model in different materials will be discussed. Moreover, the limitations of the Scholz model will also be introduced, and viable solutions to those limitations discussed.

Solid-state electrochemistry enables the study of almost any compound or material with three-dimensionally distributed, highly-concentrated redox centers,[1,2] regardless of the conductivity of oxidized or reduced forms and film thickness.[3,4] The study of varied materials in this manner is possible because the electrochemical properties can be easily measured by loading the materials onto the surface of an electrode, even in trace amounts. There are numerous methods to achieve the immobilization of solid samples to electrodes, including electrophoretic deposition,[5–8] abrasive stripping,[9] electrochemical deposition,[8] and direct growth of particles.[8] Mixing the solid sample with carbon paste or conductive polymers to form a composite electrode system is also employed.[4]

In solid-state electrochemistry, conduction is often observed as the combination of two processes: the movement of electrons between redox centers and the diffusion of counterbalancing ions to maintain a neutral charge. The electron hopping process, sometimes called redox conduction or self-exchange, is triggered by the electrolytically-generated concentration gradients arising mixed-valence redox centers in the bulk material.[1] Each of these two processes, ion diffusion or electron self-exchange, could become a potential bottleneck of the redox reaction due to the

necessity for keeping electroneutrality: the movement and accumulation of the faster species generates an electrical field, which accelerates the slower species and decelerates the faster one.[9,10]

The Cottrell equation is widely used in electrochemistry to measure diffusion (or mass transport) control over the rate of electrolysis. In the Cottrell equation (eq. 1),

$$i = \frac{nFAc\sqrt{D_{app}}}{\sqrt{\pi t}} \quad (1)$$

current is dependent on $t^{-1/2}$ because of the depletion of electroactive species near the electrode surface region.[11] In this equation, n is the number of electrons transferred in the reaction, D_{app} is the apparent diffusion coefficient, F is Faraday's constant, A is the area of electrode, t is time, and c is the concentration of redox active species.[12,13] This equation has been widely used to quantify D_{app} and solve various diffusion-related questions in many research fields, including the ion diffusion rate in solutions, diffusion-controlled electrophoretic deposition, redox hopping process in conductive polymers, across molecularly-sensitized metal oxide surfaces, and through MOFs, and more.[9,11–25]

While the Cottrell equation has been invaluable for electrochemical diffusion considerations, its weaknesses have become more apparent recently. D_{app} combines the counter ion diffusion coefficient (D_i) and electron transfer coefficient (D_e) and, therefore, lacks any acknowledgment of their individual contributions to the overall rate.[7] As aforementioned, electron hopping and counterion diffusion are interdependent and mutually restrictive processes. Thus, the slower process will become the rate-determining step for the overall process. Since optimizing the rate-determining step is the most efficient way to enhance the overall rate, it is essential to have a method that can separate the two interdependent coefficients and identify whether the rate is hindered by

electron transport or ion diffusion. The Scholz model can be used to achieve this goal and help deepen the understanding of redox hopping processes. In this perspective, we will discuss the foundational principles and assumptions of the Scholz model, experimental evidence supporting these assumptions, and practical applications of the Scholz model, along with its shortcomings.

Scholz Model. The Scholz model was first proposed to illustrate the electrochemical phenomenon in the voltammetry of microparticles (VMP).[3] As expected for a theoretical model, assumptions are made to constrain the model so that it may be solved. In the Scholz model, the main assumption is that ion insertion can only happen through the sidewall of a crystal (*0,y,z* and *x,0,z* planes) parallel to the electrode surface (Figure 1a).[3] Ion insertion from the top (x,y,z_{max}) perpendicular to the electrode surface is forbidden because it will lead to the charging of the particle-solvent interface, which cannot be directly compensated by the electrons from the electrode-crystal interface.[3]

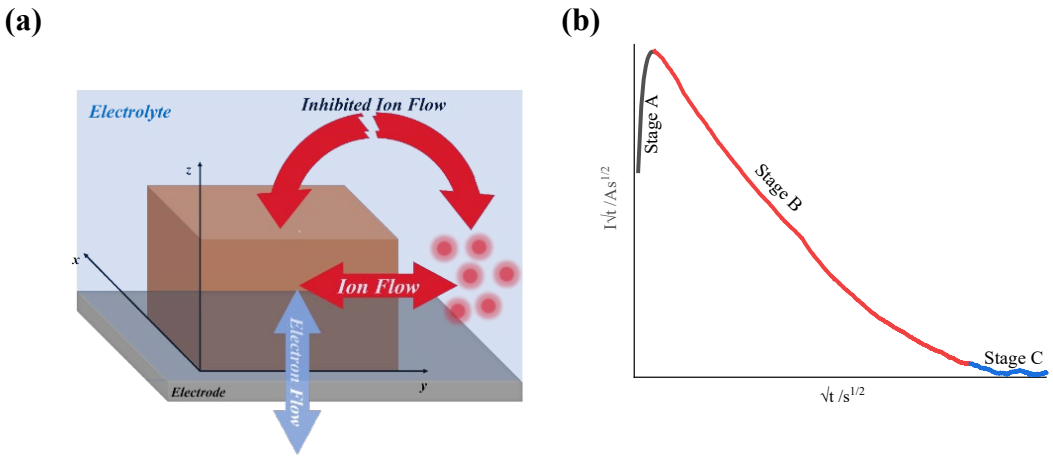

Figure 1. (a) Electron and ion movement in a solid crystal following assumptions made by the Scholz model and (b) $I\sqrt{t}$ *vs.* $\sqrt{t}$ curve with the three stages in the Scholz model.

The other key assumptions include: (1) the concentrations of the oxidized and reduced forms of electrochemically active species at the three-phase junction are governed by the Nernst equation and at thermodynamic equilibrium, and (2) the electrons move in the z-direction only (perpendicular to the electrode-crystal interface).

The ion insertion process can be divided into three distinct stages in the Scholz model: Stage A is at the onset of applied potential, in which both ion and electron diffuse unhinderedly along the interface of electrolyte and crystal into a quasi-semi-infinite space; Stage B is after all redox centers on the electrolyte-particle interface are reduced/oxidized, the reaction zone begins to penetrate the crystal bulk in this stage; and Stage C represents the very end of the reaction, treated as more than 99% of the redox centers are reduced/oxidized.[3,6,7] The way to identify the three stages is through the $I\sqrt{t}$ *vs.* $\sqrt{t}$ curve (Figure 1b): the maximum of $I\sqrt{t}$ *vs.* $\sqrt{t}$ curve correspond to the moment that all the redox centers at the electrolyte/crystal interface are converted, which marks as the end of stage A and the beginning of stage B. Stage C is generally excluded from the analysis because it is dominated by purely ion diffusion. [3,6,7]

Through the application of grid modeling and Fick's law, an equation describing the relationship between current response and time after a potential jump was developed for Stage A. By fitting experimental chronoamperometry (CA) curves with the relationship, the D_i and D_e of Stage A can be quantified. The relationship is as follows,

$$I(t) = \frac{F}{V_m}\left\{\frac{1}{1+\exp(\varphi)}\right\}\left[u\left(\left(\frac{\Delta x_0\sqrt{D_e}+\Delta z_0\sqrt{D_i}}{2\sqrt{\pi t}}\right)+\sqrt{D_e D_i}\right)-4D_i\sqrt{2D_e t}\right] \quad (2)$$

where u is the length of the three-phase junction, x_0 and z_0 represents the hopping distance of each step in the x-direction and z-direction, respectively, V_m represents the molar volume, F is the Faraday constant, D_e and D_i represent the electrons hopping coefficient and ion diffusion coefficient, respectively. φ is defined as $\varphi=E/RT(E-E_f)$ here, where E is the applied step-in potential of chronoamperometry and E_f represents the formal potential ($E^{0'}$, often estimated from the half-wave potential, $E_{1/2}$) derived from CV.

To solve the factors at the start of stage B, eq. 3 and 4 are applied.

$$t_{ref} = \frac{H^2}{1.1D_e} \tag{3}$$

$$I_{ref} = 0.72\frac{Fu}{V_m}\sqrt{D_e D_i} \tag{4}$$

where H is the height of the particles, t_{ref} and I_{ref} represent the characteristic time and the current at that time, respectively. t_{ref} and I_{ref}, are easily identified as they are the values that correspond to the maximum point in the $I\sqrt{t}$ *vs.* $\sqrt{t}$ curve. These equations can readily be applied to define the D_e and D_i parameters relevant to bulk conduction.

One important consideration is the relationship between the Scholz model and the Cotrell model and under what conditions each is derived. While both are derived from Fick's laws, there are clear differences in the physical meanings of the diffusion coefficients. To see the relationship, we use the Stage A hopping behavior, Equation 2. The standard form of Cottrell equation assumes a planar electrode, where electrons are confined to the electrode surface, i.e., they are not a diffusing species and $D_e = 0$. If we assume $D_e = 0$ in the Stage A equation, we are left with the following relation, Equation 5,

$$I(t) = \frac{F}{V_m}\left\{\frac{1}{1+\exp(\varphi)}\right\}\left[u\left(\frac{\Delta z_0\sqrt{D_i}}{2\sqrt{\pi t}}\right)\right] = u\Delta z_0 \frac{F\sqrt{D_i}}{2\sqrt{\pi t}}\frac{1}{V_m}\left\{\frac{1}{1+\exp(\varphi)}\right\} \quad (5)$$

where, the $u\Delta z_0$ term refers to the surface confined electrochemical active area around the three-phase boundary, and it is comparable to the A in the Cottrell equation, which represents the area of electrode. In the $\frac{1}{V_m}\left\{\frac{1}{1+\exp(\varphi)}\right\}$ term, the $\frac{1}{V_m}$ means the concentration of redox centers in the particle, while the $\left\{\frac{1}{1+\exp(\varphi)}\right\}$ can be transformed into $\frac{\alpha_{red}}{\alpha_{ox}+\alpha_{red}}$, which represents the ratio of reduced state of the redox center, by simply use the definition of φ. Therefore, the meaning of $\frac{1}{V_m}\left\{\frac{1}{1+\exp(\varphi)}\right\}$ is the concentration of reduced redox center, and it is comparable to the C term in the Cottrell equation. Therefore, the Scholz model in the electron confined case is equivalent to the Cottrell equation[3,27] Therefore, when one applies the Cottrell equation to a redox hopping system – there is no direct relationship between D_{app} and D_e/D_i. Indeed, the Cottrell equation assumes only one diffusing species, and thus, the resultant D_{app} for a redox hopping approach has little physical meaning. That said, the Cottrell equation is used widely in redox hopping systems due to the ease of mathematical modeling and the realization that empirically the resultant D_{app} agrees with expected trends. Indeed, in work of the Morris group, where both models were applied to the same system, the trends in D_{app} agree well with that of D_e and D_i.[6,7] That said, the lack of physical meaning to the D_{app} highlights the power of models like that of Scholz to provide a molecular context for redox hopping.

Metal Oxide Reduction. One of the most critical assumptions of the Scholz model is that the reaction starts at the three-boundary, which has been widely observed and used to explain electrochemical processes in solid-state materials, e.g., metal oxides.[28–34] The first observation of the three-phase boundary was demonstrated by Scholz through the reduction of lead oxide to lead.

In situ atomic force microscopy was applied to monitor the real-time reduction of a single α-PbO particle (Figure 2a).[31] The electrochemical reduction was performed on a gold electrode and in 1 M KCl electrolyte. Due to the volume difference between litharge (*α*-PbO) and metallic lead, the reduced metallic region will shrink and show an obvious interface, i.e., the reaction front. The reaction front region consists of lead ions and lead atoms, as well as water molecules and hydroxyl ions, which can be treated as a diffuse heterogeneous interface. By tracking the movement of the reaction front, the real-time progress of the reaction was visibly detected, and it was treated as robust evidence to prove the three-phase boundary assumption in the Scholz model.

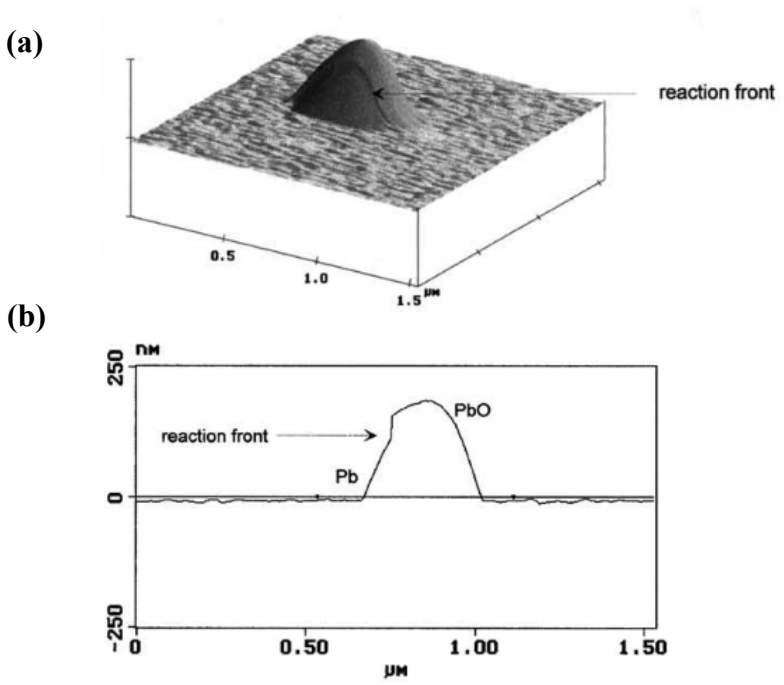

Figure 2. (a) Atomic force micrograph of an α-PbO crystal one a gold electrode in 1M KCl electrolyte after reduction for 1 s (b) 2-D crystal cross-section perpendicular to the reaction front. Reprinted with permission from ref. 31. Copyright 2001 Elsevier.

Interestingly, it was found that the reduction process starts from just one side of the detected particle instead of starting from the entire three-phase (PbO| electrolyte| gold electrode) junction of the particle (Figure 2(b)). The author proposed a few explanations for such a phenomenon: adhesion of the particle to the gold surface only occurred at the side of the reaction front, or the particle exhibited vastly anisotropic nucleation through an uncontrolled structural phenomenon. Therefore, the contact between the redox-active particle and the electrode is paramount to the measured behavior, and variability in electrode-particle contact may introduce random error in measured values. Specifically, the number of "active" particles (represented as N in the model) depends on the contact. In previous research utilizing the Scholz model, measuring the number of cuboids could become a problem. For instance, in the cases of mechanically transferring materials to the electrode, the way to determine N is from the weight of transferred materials, the dimension of cuboids, and the density.[35,36] However, the number of "active cuboids" is unknown because of the uncertain contact conditions and aggregation of the cuboids.

To solve the problem, the information derived from CA can help. By integrating the area under the CA curve, the total charge transferred in the electrochemical process can be obtained.[6,35] Knowing the concentration of the redox centers, the molar volume of the material, and the dimension of particles, the number of "active" cuboids can be derived. Such a method is especially suitable for materials with pre-determined redox center density, for example, MOFs with redox center at certain sites.[6]

Ionic Liquids. Ionic liquids (IL) are attractive materials because of their unique properties, including inflammability and nonvolatility, and have numerous applications, including batteries,

fuel cells, and capacitors.[10] Even though ILs are in the liquid state, mixing ILs with solvents in which they are immiscible results in the formation of IL drops on an electrode surface. These droplets behave similarly to tiny crystals as the properties and electrochemistry of specific IL droplets are similar to redox-active particles. Therefore, the electrochemical processes in IL can be rationalized by the Scholz model just like other redox-active solids.[37]

In the work of Schröder, the oxidation of protonated and unprotonated ionic liquids (para-N,N,N′,N′- tetrahexylphenylenediamine (THPD) and para-N,N,N′-trihexylphenylene- diamine (TriHPD)) was performed.[37] The deprotonated forms of the two ILs are electronic and ionic insulators, while the protonated forms are conductors for both. As deposited, the ILs are deprotonated and insulating. After a potential is applied, ion insertion into the IL is driven by the formation of an electric field at the electrode-droplet interface. The conductive phase is formed as the insertion process propagates. It was assumed that the reaction zone advanced as the conductive product formed, like that predicted by the Scholz model originally for porous solids (Figure 3a). For these reasons, these ILs were treated as an analog to the redox-active solids for electrochemical analysis.

When the ionic liquid exists as droplets distributed on the electrode surface or as a film not fully covering the electrode, it was found that the electrochemical oxidation was initiated at the three-phase junction (electrode | oil (ionic liquid) | aqueous solution).[37] After the electrochemical oxidation, the colored radical cation of TriHPD formed a ring about the IL droplet, which was seen via light microscopy (Figure 3b). However, the reaction was fully inhibited when the unprotonated ionic liquids were studied as a continuous film covering the whole electrode surface. The authors

concluded that the absence of a defined 3-phase boundary under full-film conditions attenuated oxidation. The implications of such findings, if proven to be consistent across other materials, are immense. Specifically, they would point to the need for grain boundaries to promote conductivity in redox hopping materials.

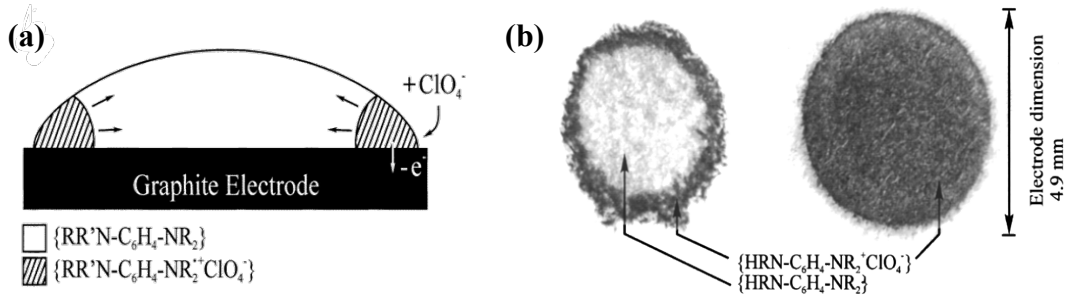

Figure 3. (a) A schematic showing the advance of reaction zone (b) Photographic image of a stamp imprint of the interlayer of unprotonated TriHPD (left) and protonated TriHPD (right) after applying a potential of 0.5 V vs. SCE for 60 s. The bright region is the unreacted ionic liquid TriHPD, and dark region is the colored TriHPD radical cation species. Reprinted with permission from ref. 37. Copyright 2001 American Chemical Society.).

While the observation of the 3-phase reaction front in IL is powerful, full quantitative application of the Scholz model is limited in the IL case. The charge transfer process includes the transition from an insulator to a conductor, which ultimately introduces a new or second 3-phase boundary as the process progresses. Moreover, the hopping distances, Δx and Δz, are not well-defined in such amorphous materials. Thus, a defined three-dimensional structure is paramount to the realization of the full potential of the Scholz model.

Organic Dyes. Human society has used organic dyes for thousands of years to achieve long-lasting coloration of fabrics. The natural properties of organic dyes make most of them redox-active. Indeed, the redox activity of organic dyes is used to produce, purify, and stabilize the dyes. The redox activity also makes the electrochemical characterization of ancient dyes possible.[38–42] Electrochemical analysis of organic dyes is generally performed in an aqueous solution, in which the dominant diffusive ion species is the proton. Therefore, in the Scholz analysis of organic dyes, the coefficient D_i is often replaced by the proton diffusion coefficient, D_H, in the literature.[35,38]

Similar to previously described systems, the three-phase boundary was observed in the organic dye nanoparticles by AFM.[31] More importantly, organic dyes represent a system amenable to quantitative analysis by the Scholz model. For example, electrochemical investigation of Maya Blue, a famous indigo-based pigment with high stability widely used in ancient wall paintings, provided insight into the oft-debated structure of the dye. One of the hypotheses is that Maya Blue consists of indigo molecules intercalated into the microporous tunnel of the inorganic mineral matrix.[43] To provide insight into the structure of Maya Blue, electrochemical characterization was performed by Doménech, et al., and the results of Maya Blue were compared with those of pure indigo, the precursor of Maya Blue.[12,36] By using the Scholz model, D_e and D_H of Maya Blue particles were calculated to be $(2 \pm 1)\times10^{-9}$ cm^2/s and $(2 \pm 1)\times10^{-8}$ cm^2/s, respectively. In indigo, D_e (3×10^{-7} cm^2/s) is faster than that in Maya Blue, while D_H (3×10^{-10} cm^2/s) is slower. The faster proton insertion rate in Maya Blue is consistent with the previous hypothesis of a porous structure in Maya Blue, which provides a favorable environment for the ion diffusion process. Additionally,

the $I\sqrt{t}$ vs. t curve from the CA study of Maya Blue particles was found to be smoother than that of indigo particles, which also provides information about the internal structure. Compared to the porous Maya Blue particles, poor ion transport across indigo nanoparticles limits the electroactive region to the external grain area and thus, leads to the fast decay of current in CA after t_{ref}.

Metal-Organic Frameworks (MOFs). Metal-organic frameworks are a family of composite materials composed of metal nodes and organic linkers. MOFs represent a rapidly growing field of solid-state materials that are known for their ordered structures, high specific surface area, high porosity, and facile structural tunability.[44,45] The development of electrically/electrochemically active MOFs for applications such as thermoelectronics, photovoltaics, semiconductors, capacitors, and electrochemical catalysts is a growing area of research.[45] Having a highly ordered and periodic geometric structure, redox-active MOFs are an excellent platform for the application of the Scholz model.

The proposed electron transfer mechanisms in MOFs include the through-bond pathway, through-plane pathway, through-space pathway, guest-promoted, and, relevant to Scholz, redox hopping.[46] Even though redox hopping has a relatively slow charge transfer rate among the aforementioned mechanisms, it has a unique advantage: the ease of MOF manipulation and design. Unlike the three "pathway" mechanisms which rely on the orbital overlap between metal ion and linker or the π-π stacking, redox hopping has lower requirements for the MOF backbone: as long as the MOF contains redox active centers, no matter if the redox center is the metal ion/cluster, the linker, or both, redox hopping is operative. For MOFs with no native redox centers, redox hopping

can also be realized by post-synthetic incorporation methods, e.g., solvent-assistant ligand incorporation (SALI).[47–51]

Table 1. Literature D_{app} values

MOF	Redox Couple	D_{app} (cm^2/s)	Ref.
Ir-UiO-66	$Ir^{III/IV}$	10^{-12}	13
Fc-MOF-808	$Fc^{+/0}$	10^{-12}	6
Fc-NU-1000	$Fc^{+/0}$	10^{-11}	6,7,20
Fc-NU-1003	$Fc^{+/0}$	10^{-11}	6
Hemin-UiO-66	$Fe^{III}P/Fe^{II}P$	10^{-9}	26
Hemin-UiO-66	$Fe^{III}P/Fe^{II}P$	10^{-10}	54
PCN-222	$Fe^{III}P/Fe^{II}P$	10^{-12}	55
MOF-525	$Fe^{III}P/Fe^{II}P$	10^{-12}	24,55
NU-902	$Fe^{III}P/Fe^{II}P$	10^{-12}	55
PCN-225	$Fe^{III}P/Fe^{II}P$	10^{-12}	55
CoPIZA	$Co^{II}P/Co^{I}P$	10^{-14}	23
NU-1000	$py^{+/0}$	10^{-10}, 10^{-13}	53
$[Ru(tpy)(dcbpy)OH_2]^{2+}$-UiO-67	$Ru^{III/II}$	10^{-9}	14
Zr(dcphOH-NDI)	$NDI^{0/\cdot-}$	10^{-9}	52

Redox hopping in MOFs has been studied in earnest since 2014, and the D_{app} derived from the Cottrell equation is treated as an important indicator of the charge transport properties of MOFs (Table 1).[6,7,13,14,20,23,24,51–54] The Cottrell equation has been applied to systems with different pore

sizes, different counter ions, different defect levels, different 3D structures, and different crystallographic orientations of MOFs.

The role of channel alignment was demonstrated by comparing the D_{app}s for vertically and horizontally aligned MOF particles (with respect to an underlying conductive substrate) (Figure 4).[53] NU-1000 prepared via solvothermal methods and electrophorectic deposition demonstrate different particle alignments. Specifically, a solvothermally prepared film results in NU-1000 particles that extend along the *c*-axis from the electrode surface. Whereas films prepared via electrophoretic deposition result in particles that lay down on the electrode along the *a,b* planes. CA analysis of films prepared via the two formation methods found that the D_{app} in NU-1000 is anisotropic, i.e., 300 times higher along *c*-axis direction than that in *a,b* plane. According to classical Marcus theory, the self-exchange rate for electrons should increase when the distance between hopping centers is decreased. The governing factor of anisotropy in NU-1000 was attributed to the difference in linker-to-linker distance and electronic coupling in different directions, which is a direct consequence of NU-1000's lower crystalline symmetry.

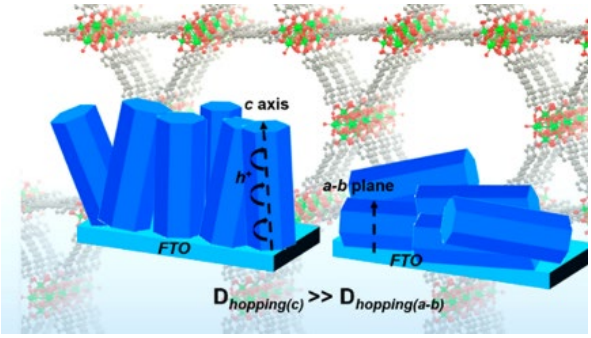

Figure 4. The anisotropic charge transfer along c-axis and in *a,b* plane of NU-1000. Reprinted from ref. 53. Copyright 2019 American Chemical Society.

A similar phenomenon is borne out in studies of MOFs with different concentrations of redox-hopping centers. For example, the concentration of redox-hopping centers (and by proxy the distance and electronic coupling between those centers) was explored in $[Ru(tpy)(dcbpy)OH_2]^{2+}$-UiO-67 (tpy = 2,2′:6′,2′′-terpyridine, dcbpy = 5,5′-dicarboxy-2,2′-bipyridine) thin films.[14] As the concentration was increased from ~1 x 10^{-10} mol/cm^2 to 1 x 10^{-8} mol/cm^2, a shift from surface-limited electrochemistry to redox hopping through the entire film was observed. The same phenomenon was explored in post-synthetically modified UiO-66 films with Hemin as a redox active center.[26] Interestingly, the Hemin@UiO-66 sample with the lowest defect density exhibited the highest D_{app} (4 x 10^{-9} cm^2/sec, compared to 0.36 x 10^{-9} cm^2/sec at the highest defect density). The authors rationalized the observation from the localization of the Hemin molecules throughout the 3D framework. At low defect densities, the Hemin was hypothesized to be primarily located on the external surface of the MOF particles. Whereas, at high defect density, a more homogeneous distribution of Hemin throughout the 3D structure was possible. Thus, the distance between the hopping centers is smallest for the low defect density material and the fastest hopping rate observed. It is important to note that in classic redox hopping behavior for molecules attached to the surface of metal oxide nanoparticles, the observation of a percolation threshold, defined as the critical concentration needed to support a hopping mechanism, is often observed through a detailed concentration analysis.[18,56] In such experiments, once the critical concentration is reached a dramatic increase in the D_{app} is observed. In both concentration-dependent studies discussed here, a percolation threshold was not observed in MOFs and points to the complexity that the 3D distribution of redox centers imparts in observed behavior.

As mentioned, the Cottrell equation and, thus D_{app}, lack the ability to separate the contributions from electron diffusion and ion diffusion.[7] The disentanglement of D_e and D_i becomes a necessity to rationally deepen the understanding, improve the charge transfer, and optimize the design of redox-active MOFs. The Scholz model provides a possible means to achieve this goal.

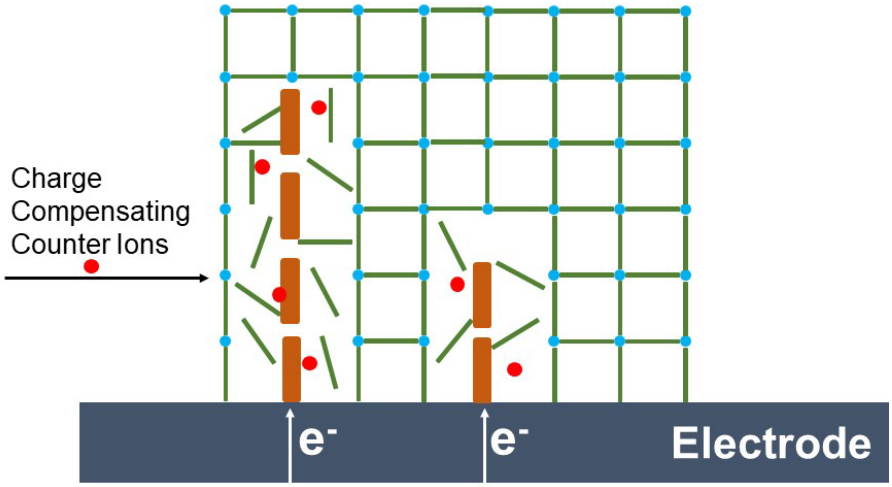

Figure 5. A Schematic showing the formation of copper metal laminas intercalated in the MOF after reduction. The blue dots and green rods represent for copper nodes and organic linkers, respectively, and the brown chunks represents the metallic copper with a laminar structure. Reprinted with permission from ref 57. Copyright © 2006 Elsevier.

The Scholz model was first applied in the work of Domenech et al.,[57] to demonstrate the electrochemical reduction of the metal nodes of a MOF. A negative potential was applied to a copper-based MOF, and the native Cu^{2+} node was reduced to Cu^{+} and, subsequently, Cu^{0}. Upon reduction to Cu^{0} the nodes decomposed and formed metallic copper particles. The copper metal particles formed laminas intercalated in the framework (Figure 5). The laminar structure of metallic

copper was attributed to the charge transfer following preferential direction, which was rationalized by the direction of electron and ion motion set forth by the Scholz model. In addition, the orientation of the metal laminas (perpendicular to the electrode surface, in the electron hopping direction) suggests that electron hopping is much faster than ion diffusion. Even though this work did not give quantitative analysis regarding redox hopping, it did support the applicability of the Scholz model to MOFs and indicate that the electron hopping is much faster than the ion diffusion in the system.

The first quantitative application of the Scholz model was carried out by Celis-Salazar et al. for metallocene-doped NU-1000 (M-NU-1000).[7] It was found that the D_es of doped M-NU-1000s increased in the following the order ferrocene < ruthenocene < osmocene, which is consistent with the self-exchange rate of the M^{2+}/M^{3+} (M=Fe, Ru, Os) couples. Meanwhile, D_i was found to be dependent on three factors: MOF's pore size, counter ion size, and the ion-pairing ability (discussed in the following paragraphs). Importantly, in all quantitative studies to date, the D_e values are higher than that of D_i often by several orders of magnitude. Thus, it is the diffusion of ions that limits the overall redox hopping conductivity in MOFs.

The ability to quantify D_e and D_i as a function of the Scholz model stages enabled further confirmation for the difference in hopping rate as a function of redox active molecule distribution. As previously discussed, D_{app} analysis of UiO-66@Hemin samples indicated that molecules restricted to the surface of the particles are reduced and oxidized faster than those in the interior of the MOF particle. For M-NU-1000 MOFs, the D_e values were three- to four- orders of magnitude faster during Stage A (when the exterior of the MOF is oxidized) versus Stage B (when molecules

in the MOF interior are oxidized). The observation was attributed to the reduced degrees of freedom available to the interior metallocene centers and consequently, a more fixed and larger distance between the redox active molecules.

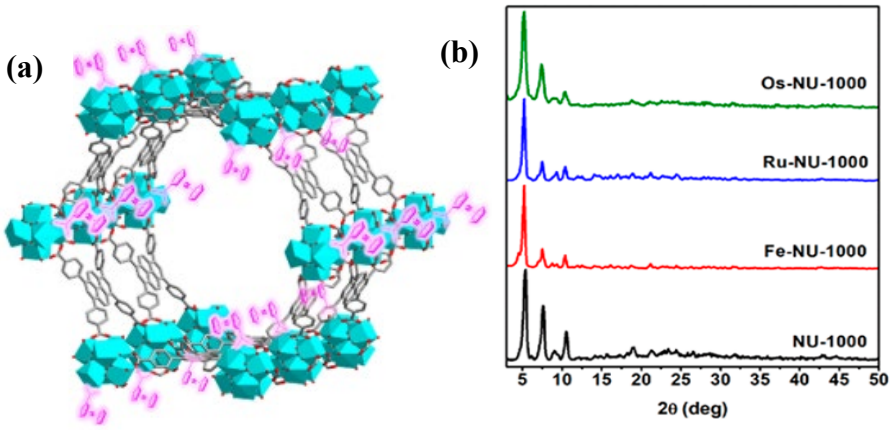

Figure 6. (A) The schematic of MOF modified with redox hopping center on the metal nodes (B) PXRD pattern of unmodified MOF and MOFs modified through post-synthetic method (SALI). Reprinted with permission from refs 7. Copyright © 2019 American Chemical Society.

The relationship between dimensional properties of ferrocene (Fc)-doped MOFs and charge transfer were explored by Cai et al..[6] It was found that increases in pore size from 15 to 47 $\AA$ for a series of Fc-doped MOFs, Fc-MOF-808, Fc-NU-1000, and Fc-NU-1003, (Figure 7) lead to a negative effect on electron hopping. Indeed, the electron transfer rate constant ($k_{e\text{-}hop}$, derived from $k_{e-hop} = \frac{D_e}{r^2}$, where r is the hopping distance) decreased from ~3 x 10^7 s^{-1} to 0.90 x 10^7 s^{-1} in Stage A and ~8 x 10^3 s^{-1} to 2 x 10^3 s^{-1} in Stage B. Like the concentration effect, the increase in the hopping distance between redox centers as a function of pore size would result in decreased

electronic coupling. Conversely, the increase in pore size had a positive effect on the ion diffusion process due to the larger transport channels available. The values for $k_{i\text{-}hop}$ increased 1-2 orders of magnitude while pore size increased (e.g., 0.5 s^{-1} to 43 s^{-1} for tetrakis(pentafluorophenyl)borate ion, $TFAB^-$). Overall, the D_{app}s derived from the Cottrell equation of the three MOFs were found to increase with the MOF's pore size, indicating that the enlargement of pore size improves the overall rate of redox-hopping process and providing support that the ion diffusion is the rate-determining step. A similar observation was observed for a series of topologically variant porphyrin MOFs,[55,58] supporting the application of the principle over a wide range of MOFs with different redox active centers and incorporation methods.

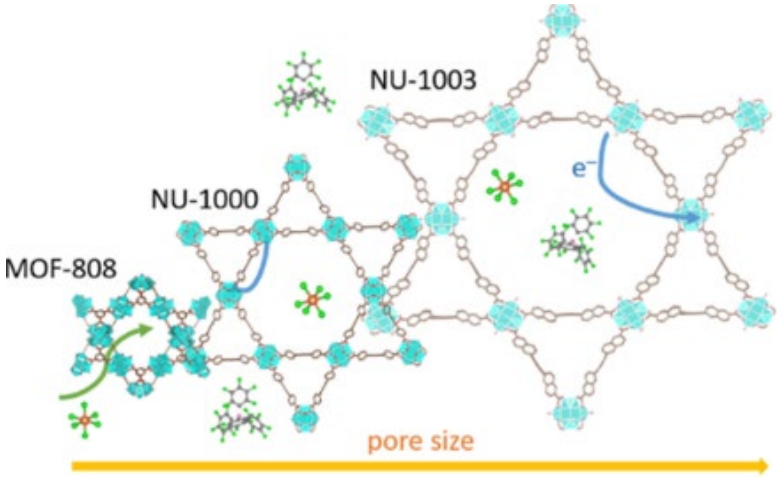

Figure 7. Schematic structures of MOF-808, NU-1000, and NU-1000 showing the change in size of the hexagonal pores. Reprinted with permission from refs 6. Copyright © 2020 American Chemical Society.

The effect of ion size was also explored in NU-1000 and Fc-NU-1000. For native NU-1000, switching the counter ion from hexafluorophosphate (PF_6^-) to tetrakis[3,5-bis(trifluoromethyl)

phenyl] borate ($BARF^-$) engenders a two- to four- fold decrease in D_{app} for solvothermally-prepared films.[59] The diameters of PF_6^- and $BARF^-$ are 5 *Å* and 15 *Å*, respectively, and the pore sizes of NU-1000 are ~30 *Å* for hexagonal pores and 12 *Å* for triangular pores. Therefore, one could attribute the difference in D_{app} to the relative ratio of the anion to the pores with smaller anions transporting through the pores faster. However, in Fc-NU-1000 films, the trend observed was the opposite. Specifically, tetrakis(pentafluorophenyl)borate ion ($TFAB^-$) has higher D_i than hexafluorophosphate ion (PF_6^-).[7] The observation was attributed to the weaker ion-paring interaction between $TFAB^-$ and the metallocene center, even though $TFAB^-$ is bulkier than PF_6^-. The comparison of the behavior of NU-1000 to that of Fc-NU-1000 implicates a complicated balance between the size of the counter-balancing ion and its ion pairing ability. The conditions under which each parameter dictates behavior require further investigation. Further investigation is particularly relevant given that EPD-prepared NU-1000 films did not show dependence on the size of the counterion.

While there have been several studies that qualitatively or quantitatively applied the Scholz model to comprehend electrochemical phenomena in solid-state materials, it is important to recognize that a theoretical model cannot account for all experimental nuances. Two of the major limitations elaborated throughout this review are: (1) the importance of the particle electrode contact, and (2) the complications that arise from non-homogeneous distributions of redox centers.

As observed in the α-PbO case, the connection between the particles and the electrode is paramount to observed redox processes. Specifically, poor electrode contact was hypothesized to cause in-homogeneous reduction of the α-PbO, i.e., from only one three phase boundary. The

limitation exposes the importance of the resistance at the particle-electrode interface and that in the application of the Scholz model, one must assume that to be low in comparison to in-particle transport. If that were not the case, the CA response would simply report on that interfacial resistance – and little-to-no useful data about in-particle redox hopping would be uncovered. The effect is particularly important and relevant to film preparation methods that are uncontrolled, e.g., solvothermal growth of MOF particles and EPD deposition of MOF particles. Expanding beyond the electrode-particle interface, resistance effects at particle-particle interfaces for multi-layer films would also complicate analysis by the Scholz mode. Therefore, care should be taken for deposited films to be thin, at a minimum, and single particle thick, if possible.

As a natural extension to a controlled particle-electrode contact, the dimension of the three-phase junction of the particles must be known and well-defined to calculate the D_e and D_i. For MOFs, like NU-1000, MOF-808, and PCN-222, with controlled growth or deposition geometries, the particles naturally have preferred face(s) that contact the electrode. Thus, the length of the three-phase junction is well-defined and can be determined via microscopy easily. However, for MOFs with more complicated morphologies, determining the dimensions of the three-phase junction is difficult. For example, in the Zr- or Hf-based MOF DUT-67, with both regular hexagonal and square crystal planes, the length of three-phase junction is unclear (Figure 8).[60] Considering the increasing number of MOFs utilized in electrochemistry and over 30,000 known MOF structures, the need to measure the electrochemical responses of more complex MOF structures is imminent. One possible solution is to use the weighted average length of all possible three-phase junctions.

Depending on the method of deposition, the weighted average may change but it is still possible to be determined by SEM images.

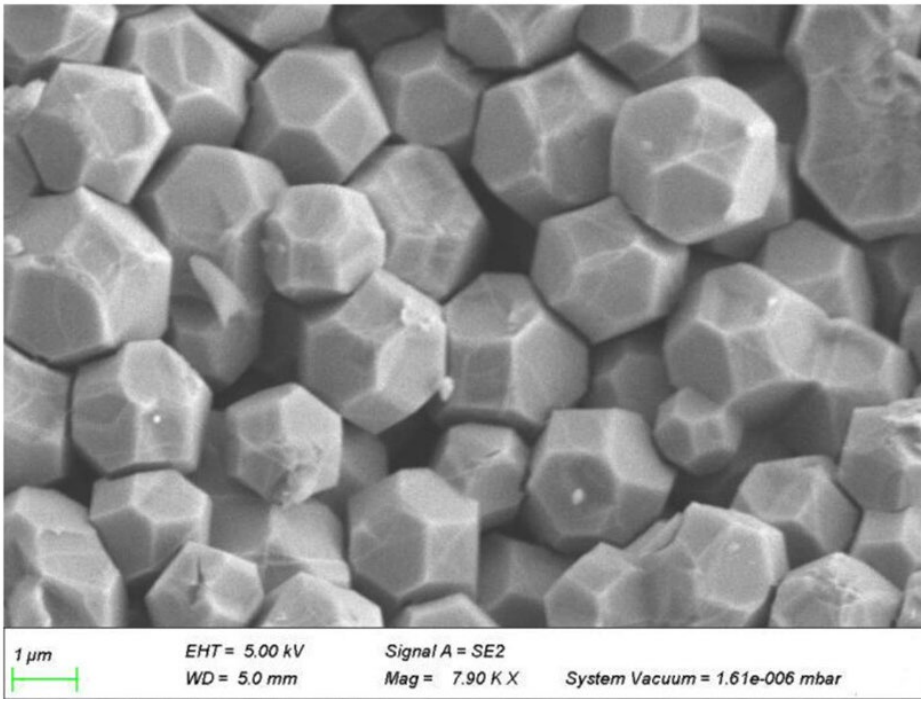

Figure 8. Representative SEM images of Hf-DUT-67 showing the regular hexagonal and square faces. Reprinted with permission from refs 60. Copyright © 2023 American Chemical Society.

Redox hopping research on MOFs has brough to the forefront the expected dependence of electron hopping on the distance between active sites. Indeed, it was shown that molecules on the surface of particles, as observed in Stage A of the Scholz progression, exhibit higher D_es than those in the MOF interior. Therefore, materials with non-crystallographic arrangements (and potential even those with crystallographic arrangements) of redox active species should display a distribution

of D_e (and D_i) values, a fact that builds significant error into reported values. A more rigorous analysis would account for and report the distributions – is it a Gaussian distribution? A stretched exponential function? Efforts should be placed on the development of synthetic conditions to promote reproducibility in structure, including post-synthetically added molecules. Additionally, characterization methods that can accurately visualize the distribution of such additives should be advanced.

The earliest and arguably most powerful support for the Scholz model came from visualization of the three-phase boundary and propagation pathways for ions/electrons. That said, two of the materials exploited for this purpose, metal oxides and ionic liquid, are not pure redox-active solids. The conduction mechanism in each requires the generation of another reaction front or conductive pathway – through metal deposition or protonation. Additionally, the primary method used for reaction tracking – AFM – is not readily applicable to electrochemically-stable MOFs. AFM required a volume difference before and after the redox reaction, which is not common in all solid-state materials. For example, in the organic dye, Maya Blue, the rigid matrix nature leads to negligible volume change during the redox reaction. Therefore, AFM is not a practical way to monitor the real-time redox process happening in many materials.

In the IL example, visual microscopy was used to visualize the initiation of reactivity at the three-phase boundary. The expansion of such spectroscopic visualization methods that cannot only provide snap-shot support for three-phase boundaries and propagation, but also have the potential to be expanded to real-time tracking are of particular interest for future development. Through visualized redox reactions, the complications described above, e.g., inconsistency of the electrode-

particle interface and potential multi-layer propagation, can be accounted for through experimental design. Measurement of numerous particles via a visualization method may also provide a more quantitative view of the role of inhomogeneous redox active molecule inclusion.

To summarize, the Scholz model has provided explanations for various phenomena regarding electrochemical processes in solid-state materials and analogous systems. Moreover, it provides both a qualitative framework for scientists to rationalize observations relevant to the propagation directions for electron and ion motion in redox solids, but also, a quantitative method to determine the impact of ion and electron motion to overall conductivity. So far, the findings derived from the Scholz model that contribute to the fields understanding of redox hopping include:

(1) Redox hopping processes originate and propagate from the electrode-particle-solvent, or three-phase boundary. The direction of propagation depends on whether electron transport (horizontal to the electrode) or ion transport (perpendicular to the electrode) is rate limiting.

(2) Application of the Scholz model can be used to decipher the three-dimensional nature of a material. As demonstrated with organic dyes, the porous structure of Maya Blue was confirmed by comparison of the hopping rate to a non-porous analog.

(3) The three-phase boundary is necessary for redox conduction, as demonstrated in ionic liquids. The results imply that grain boundaries or individual particles may be required for redox hopping to be operative.

(4) In redox-hopping MOFs, ion diffusion is the bottleneck for the charge transfer process in all the systems explored to date. Indeed, the difference between D_e and D_i is orders of magnitude.

(5) The pore size of MOFs can affect both D_e and D_i. Nevertheless, in most cases, considering that D_i is orders of magnitude smaller than D_e, larger pore size leads to higher overall charge transport performance.

These findings highlight the impact analysis by the Scholz model has in redox hopping material design. That said, there are numerous additional avenues for future exploration, such as: Can the application of the model be expanded to other redox active solids, i.e., battery materials and/or perovskites? Can we eliminate or correct deviations resulting from these heterogeneities in electrode contact or redox-active molecule distribution through visualization methods? Can we apply the model *a priori* to predict the redox hopping behavior of MOFs based on the information on the redox center, MOF structure, and morphological features of MOFs? The answers to these questions will lead to a broader application of the Scholz model, a deeper understanding of redox hopping processes and, consequently, more strategies to improve charge transfer in porous materials.

Author Information

Corresponding Author

Amanda J. Morris – Department of Chemistry, Virginia Polytechnic Institute and State University, Blacksburg, Virginia 24061-0131, United States

*Email: ajmorris@vt.edu

Authors

Minliang Yan - Macromolecules Innovation Institute, Virginia Polytechnic Institute and State University, Blacksburg, Virginia 24061-0131, United States

Eric M. Johnson - Department of Chemistry, Virginia Polytechnic Institute and State University, Blacksburg, Virginia 24061-0131, United States

Acknowledgement

M. Y. is supported by the National Science Foundation under Grant No. DMR-2109934.

Reference

(1) Kulesza, P. J.; Cox, J. A. Solid-State Voltammetry - Analytical Prospects. *Electroanalysis* **1998**, *10* (2), 73–80.

(2) Mohammad-Pour, G. S.; Hatfield, K. O.; Fairchild, D. C.; Hernandez-Burgos, K.; Rodríguez-López, J.; Uribe-Romo, F. J. A Solid-Solution Approach for Redox Active Metal-Organic Frameworks with Tunable Redox Conductivity. *J. Am. Chem. Soc.* **2019**, *141* (51), 19978–19982.

(3) Schröder, U.; Oldham, K. B.; Myland, J. C.; Mahon, P. J.; Scholz, F. Modelling of Solid State Voltammetry of Immobilized Microcrystals Assuming an Initiation of

the Electrochemical Reaction at a Three-Phase Junction. *J. Solid State Electrochem.* **2000**, *4* (6), 314–324.

(4) Bond, A. M. *Broadening Electrochemical Horizons: Principles and Illustration of Voltammetric and Related Techniques*; Oxford University Press: New York, 2002.

(5) Hod, I.; Bury, W.; Karlin, D. M.; Deria, P.; Kung, C. W.; Katz, M. J.; So, M.; Klahr, B.; Jin, D.; Chung, Y. W.; Odom, T. W.; Farha, O. K.; Hupp, J. T. Directed Growth of Electroactive Metal-Organic Framework Thin Films Using Electrophoretic Deposition. *Adv. Mater.* **2014**, *26* (36), 6295–6300.

(6) Cai, M.; Loague, Q.; Morris, A. J. Design Rules for Efficient Charge Transfer in Metal-Organic Framework Films: The Pore Size Effect. *J. Phys. Chem. Lett.* **2020**, *11* (3), 702–709.

(7) Celis-Salazar, P. J.; Cai, M.; Cucinell, C. A.; Ahrenholtz, S. R.; Epley, C. C.; Usov, P. M.; Morris, A. J. Independent Quantification of Electron and Ion Diffusion in Metallocene-Doped Metal-Organic Frameworks Thin Films. *J. Am. Chem. Soc.* **2019**, *141* (30), 11947–11953.

(8) Genesio, G.; Maynadié, J.; Carboni, M.; Meyer, D. Recent Status on MOF Thin Films on Transparent Conductive Oxides Substrates (ITO or FTO). *New J. Chem.* **2018**, *42* (4), 2351–2363.

(9) Lovrić, M.; Scholz, F. A Model for the Propagation of a Redox Reaction through Microcrystals. *J. Solid State Electrochem.* **1997**, *1* (1), 108–113.

(10) Weaver, J. E. F.; Breadner, D.; Deng, F.; Ramjee, B.; Ragogna, P. J.; Murray, R. W. Electrochemistry of Ferrocene-Functionalized Phosphonium Ionic Liquids. *J. Phys. Chem. C* **2011**, *115* (39), 19379–19385.

(11) Bard, A. J.; Faulkner, L. R. *Electrochemical Methods——Fundamentals and Applications*; John Wiley & Sons, Inc.,: New York, 2000.

(12) Doménech, A.; Doménech-Carbó, M. T.; De Agredos Pascual, M. L. V. Indigo/Dehydroindigo/Palygorskite Complex in Maya Blue: An Electrochemical Approach. *J. Phys. Chem. C* **2007**, *111* (12), 4585–4595.

(13) Chuang, C. H.; Li, J. H.; Chen, Y. C.; Wang, Y. Sen; Kung, C. W. Redox-Hopping and Electrochemical Behaviors of Metal−organic Framework Thin Films Fabricated by Various Approaches. *J. Phys. Chem. C* **2020**, *124* (38), 20854–20863.

(14) Lin, S.; Pineda-Galvan, Y.; Maza, W. A.; Epley, C. C.; Zhu, J.; Kessinger, M. C.; Pushkar, Y.; Morris, A. J. Electrochemical Water Oxidation by a Catalyst-Modified Metal–Organic Framework Thin Film. *ChemSusChem* **2017**, *10* (3), 514–522.

(15) Zhang, J.; Bond, A. M. Conditions Required to Achieve the Apparent Equivalence of Adhered Solid- and Solution-Phase Voltammetry for Ferrocene and Other Redox-Active Solids in Ionic Liquids. *Anal. Chem.* **2003**, *75* (11), 2694–2702.

(16) Karlsson, C.; Suga, T.; Nishide, H. Quantifying TEMPO Redox Polymer Charge Transport toward the Organic Radical Battery. *ACS Appl. Mater. Interfaces* **2017**, *9* (12), 10692–10698.

(17) Khoo, E.; Lee, P. S.; Ma, J. Electrophoretic Deposition (EPD) of WO3 Nanorods for Electrochromic Application. *J. Eur. Ceram. Soc.* **2010**, *30* (5), 1139–1144.

(18) Trammell, S. A.; Yang, J.; Sykora, M.; Fleming, C. N.; Odobel, F.; Meyer, T. J. Molecular Energy Transfer across Oxide Surfaces. *J. Phys. Chem. B* **2001**, *105* (37), 8895–8904.

(19) Staniszewski, A.; Morris, A. J.; Ito, T.; Meyer, G. J. Conduction Band Mediated Electron Transfer across Nanocrystalline TiO 2 Surfaces. *J. Phys. Chem. B* **2007**, *111* (24), 6822–6828.

(20) Hod, I.; Farha, O. K.; Hupp, J. T. Modulating the Rate of Charge Transport in a Metal-Organic Framework Thin Film Using Host:Guest Chemistry. *Chem. Commun.* **2016**, *52* (8), 1705–1708.

(21) Palmer, R. H.; Liu, J.; Kung, C. W.; Hod, I.; Farha, O. K.; Hupp, J. T. Electroactive Ferrocene at or near the Surface of Metal-Organic Framework UiO-66. *Langmuir* **2018**, *34* (16), 4707–4714.

(22) Sun, L.; Jiao, K.; Weber, S. G. Charge Transport through Osmium-Containing Redox Polymers in Nitrophenyl-Based Solvents: Effect of Solvent Size. *J. Phys. Chem. B* **1998**, *102* (11), 1945–1950.

(23) Ahrenholtz, S. R.; Epley, C. C.; Morris, A. J. Solvothermal Preparation of an Electrocatalytic Metalloporphyrin MOF Thin Film and Its Redox Hopping Charge-Transfer Mechanism. *J. Am. Chem. Soc.* **2014**, *136* (6), 2464–2472.

(24) Kung, C. W.; Chang, T. H.; Chou, L. Y.; Hupp, J. T.; Farha, O. K.; Ho, K. C. Porphyrin-Based Metal-Organic Framework Thin Films for Electrochemical Nitrite Detection. *Electrochem. commun.* **2015**, *58*, 51–56.

(25) Montella, C. Discussion of the Potential Step Method for the Determination of the Diffusion Coefficients of Guest Species in Host Materials: Part I. Influence of Charge Transfer Kinetics and Ohmic Potential Drop. *J. Electroanal. Chem.* **2002**, *518* (2), 61–83.

(26) Shimoni, R.; He, W.; Liberman, I.; Hod, I. Tuning of Redox Conductivity and Electrocatalytic Activity in Metal-Organic Framework Films Via Control of Defect Site Density. *J. Phys. Chem. C* **2019**, *123* (9), 5531–5539.

(27) Doménech, A.; Doménech-Carbó, M. T.; Del Río, M. S.; De Agredos Pascual, M. L. V. Comparative Study of Different Indigo-Clay Maya Blue-like Systems Using the Voltammetry of Microparticles Approach. *J. Solid State Electrochem.* **2009**, *13* (6), 869–878.

(28) Doménech-Carbó, A.; Dias, D.; Doménech-Carbó, M. T. Cation and Anion Electrochemically Assisted Solid-State Transformations of Malachite Green. *Phys. Chem. Chem. Phys.* **2020**, *22* (3), 1502–1510.

(29) Doménech-Carbó, A.; Sabaté, F.; Sabater, M. J. Electrochemical Analysis of Catalytic and Oxygen Interfacial Transfer Effects on MnO2 Deposited on Gold Electrodes. *J. Phys. Chem. C* **2018**, *122* (20), 10939–10947.

(30) Redondo-Marugán, J.; Piquero-Cilla, J.; Doménech-Carbó, M. T.; Ramírez-Barat, B.; Sekhaneh, W. Al; Capelo, S.; Doménech-Carbó, A. Characterizing Archaeological Bronze Corrosion Products Intersecting Electrochemical Impedance Measurements with Voltammetry of Immobilized Particles. *Electrochim. Acta* **2017**, *246*, 269–279.

(31) Hasse, U.; Scholz, F. In Situ Atomic Force Microscopy of the Reduction of Lead Oxide Nanocrystals Immobilised on an Electrode Surface. *Electrochem. commun.* **2001**, *3* (8), 429–434.

(32) Doménech-Carbó, A.; Doménech-Carbó, M.; Martínez-Lázaro, I. Electrochemical Identification of Bronze Corrosion Products in Archaeological Artefacts. A Case Study. *Microchim. Acta* **2008**, *162* (3–4), 351–359.

(33) Taviot-Guého, C.; Vialat, P.; Leroux, F.; Razzaghi, F.; Perrot, H.; Sel, O.; Jensen, N. D.; Nielsen, U. G.; Peulon, S.; Elkaim, E.; Mousty, C. Dynamic Characterization of Inter- and Intralamellar Domains of Cobalt-Based Layered Double Hydroxides upon Electrochemical Oxidation. *Chem. Mater.* **2016**, *28* (21), 7793–7806.

(34) Komorsky-Lovrić, Š.; Lovrić, M.; Scholz, F. Square-Wave Voltammetry of Decamethylferrocene at the Three-Phase Junction Organic Liquid/Aqueous Solution/Graphite. *Collect. Czechoslov. Chem. Commun.* **2001**, *66* (3), 434–444.

(35) Domenech, A.; Domenech-Carbo, M. T. Chronoamperometric Study of Proton Transfer / Electron Transfer in Solid State Electrochemistry of Organic Dyes. *J Solid State Electrochem* **2006**, *10*, 949–958.

(36) Doménech, A.; Doménech-Carbó, M. T.; De Agredos Pascual, M. L. V. Dehydroindigo: A New Piece into the Maya Blue Puzzle from the Voltammetry of Microparticles Approach. *J. Phys. Chem. B* **2006**, *110* (12), 6027–6039.

(37) Schröder, U.; Compton, R. G.; Marken, F.; Bull, S. D.; Davies, S. G.; Gilmour, S. Electrochemically Driven Ion Insertion Processes across Liquid Liquid

Boundaries: Neutral versus Ionic Redox Liquids. *J. Phys. Chem. B* **2001**, *105* (7), 1344–1350.

(38) Doménech, A.; Doménech-Carbó, M. T.; De Agredos Pascual, M. L. V. Electrochemical Monitoring of Indigo Preparation Using Maya's Ancient Procedures. *J. Solid State Electrochem.* **2007**, *11* (9), 1335–1346.

(39) Chethana, B. K.; Basavanna, S.; Naik, Y. A. Electrochemical Studies on Lawsone and Its Determination in Henna (Lawsonia Inermis) Extract Using Glassy Carbon Electrode. *J. Anal. Chem.* **2014**, *69* (9), 887–891.

(40) Doménech-Carbó, A.; Doménech-Carbó, T.; Saurí-Peris, C.; Gimeno-Adelantado, J. V.; Bosch-Reig, F. Identification of Curcuma and Safflower Dyes by Voltammetry of Microparticles Using Paraffin-Impregnated Graphite Electrodes. *Microchim. Acta* **2005**, *152* (1–2), 75–84.

(41) Doménech-Carbó, A.; Doménech-Carbó, M. T.; Calisti, M.; Maiolo, V. Identification of Naphthoquinonic and Anthraquinonic Dyes via Sequential Potential Steps Applied to the Voltammetry of Microparticles Methodology. *J. Solid State Electrochem.* **2010**, *14* (3), 465–477.

(42) Doménech-Carbó, A.; Doménech-Carbó, M. T.; Osete-Cortina, L.; Valle-Algarra, F. M.; Buti, D. Isomerization and Redox Tuning in "Maya Yellow" Hybrids from

Flavonoid Dyes plus Palygorskite and Kaolinite Clays. *Microporous Mesoporous Mater.* **2014**, *194*, 135–145.

(43) Fernández-Sabido, S.; Palomo-Carrillo, Y.; Burgos-Villanueva, R.; De Coss, R. Comparative Study of Two Blue Pigments from the Maya Region of Yucatan. *Mater. Res. Soc. Symp. Proc.* **2012**, *1374*, 115–123.

(44) Mondloch, J. E.; Karagiaridi, O.; Farha, O. K.; Hupp, J. T. Activation of Metal – Organic Framework Materials. *Cryst Eng Comm* **2013**, *15*, 9258–9264.

(45) Lin, S.; Usov, P. M.; Morris, A. J. The Role of Redox Hopping in Metal-Organic Framework Electrocatalysis. *Chem. Commun.* **2018**, *54* (51), 6965–6974.

(46) Johnson, E. M.; Ilic, S.; Morris, A. J. Design Strategies for Enhanced Conductivity in Metal-Organic Frameworks. *ACS Cent. Sci.* **2021**, *7* (3), 445–453.

(47) Nagatomi, H.; Gallington, L. C.; Goswami, S.; Duan, J.; Chapman, K. W.; Yanai, N.; Kimizuka, N.; Farha, O. K.; Hupp, J. T. Regioselective Functionalization of the Mesoporous Metal−Organic Framework, NU-1000, with Photo-Active Tris-(2,2′bipyridine)Ruthenium(II). *ACS Omega* **2020**, *5* (46), 30299–30305.

(48) Duan, J.; Goswami, S.; Hupp, J. T. Redox-Hopping-Based Charge Transport Mediated by Ru(II)-Polypyridyl Species Immobilized in a Mesoporous Metal-Organic Framework. *Front. Chem. Eng.* **2022**, *3* (February), 1–6.

(49) Deria, P.; Bury, W.; Hupp, J. T.; Farha, O. K. Versatile Functionalization of the Nu-1000 Platform by Solvent-Assisted Ligand Incorporation. *Chem. Commun.* **2014**, *50* (16), 1965–1968.

(50) Oh, J. S.; You, Y.; Park, K. C.; Gupta, G.; Kang, D. K.; Lee, C. Y. Toward an Efficient Photosensitizer for Photodynamic Therapy: Incorporating BODIPY into Porphyrinic Nanoscale MOFs through the Solvent-Assisted Ligand Incorporation. *Dye. Pigment.* **2019**, *170* (May), 107576.

(51) Deria, P.; Bury, W.; Hod, I.; Kung, C. W.; Karagiaridi, O.; Hupp, J. T.; Farha, O. K. MOF Functionalization via Solvent-Assisted Ligand Incorporation: Phosphonates vs Carboxylates. *Inorg. Chem.* **2015**, *54* (5), 2185–2192.

(52) Castner, A. T.; Su, H.; Svensson Grape, E.; Inge, A. K.; Johnson, B. A.; Ahlquist, M. S. G.; Ott, S. Microscopic Insights into Cation-Coupled Electron Hopping Transport in a Metal-Organic Framework. *J. Am. Chem. Soc.* **2022**, *144* (13), 5910–5920.

(53) Goswami, S.; Hod, I.; Duan, J. D.; Kung, C. W.; Rimoldi, M.; Malliakas, C. D.; Palmer, R. H.; Farha, O. K.; Hupp, J. T. Anisotropic Redox Conductivity within a Metal-Organic Framework Material. *J. Am. Chem. Soc.* **2019**, *141* (44), 17696–17702.

(54) Liberman, I.; Shimoni, R.; Ifraemov, R.; Rozenberg, I.; Singh, C.; Hod, I. Active-Site Modulation in an Fe-Porphyrin-Based Metal-Organic Framework through Ligand Axial Coordination: Accelerating Electrocatalysis and Charge-Transport Kinetics. *J. Am. Chem. Soc.* **2020**, *142* (4), 1933–1940.

(55) Maindan, K.; Li, X.; Yu, J.; Deria, P. Controlling Charge-Transport in Metal-Organic Frameworks: Contribution of Topological and Spin-State Variation on the Iron-Porphyrin Centered Redox Hopping Rate. *J. Phys. Chem. B* **2019**, *123* (41), 8814–8822.

(56) Papageorgiou, N.; Grätzel, M.; Enger, O.; Bonifazi, D.; Diederich, F. Lateral Electron Transport inside a Monolayer of Derivatized Fullerenes Anchored on Nanocrystalline Metal Oxide Films. *J. Phys. Chem. B* **2002**, *106* (15), 3813–3822.

(57) Doménech, A.; García, H.; Doménech-Carbó, M. T.; Llabrés-i-Xamena, F. Electrochemistry Nanometric Patterning of MOF Particles: Anisotropic Metal Electrodeposition in Cu/MOF. *Electrochem. commun.* **2006**, *8* (12), 1830–1834.

(58) Rajasree, S. S.; Li, X.; Deria, P. Physical Properties of Porphyrin-Based Crystalline Metal–organic Frameworks. *Commun. Chem.* **2021**, *4* (1), 1–14.

(59) Duan, J.; Goswami, S.; Patwardhan, S.; Hupp, J. T. Does the Mode of Metal-Organic Framework/Electrode Adhesion Determine Rates for Redox-Hopping-

Based Charge Transport within Thin-Film Metal-Organic Frameworks? *J. Phys. Chem. C* **2022**, *126* (9), 4601–4611.

(60) Kang, L. L.; Xing, C.; Jin, Y. X.; Xie, L. X.; Li, Z. F.; Li, G. Two Dual-Function Zr/Hf-MOFs as High-Performance Proton Conductors and Amines Impedance Sensors. *Inorg. Chem.* **2023**, *62* (7), 3036–3046.

Author biography:

Minliang Yan is pursuing his doctoral studies as a PhD candidate in the Macromolecular Science and Engineering program at the Macromolecules Innovation Institute of Virginia Tech. He completed his undergraduate education with a bachelor's degree in Polymer Materials and Engineering from Central South University in 2017. Advancing his expertise, he earned his master's degree in Materials Engineering from the University of Southern California in 2020. That same year marked the beginning of his research in the team led by Professor Amanda Morris. He is focusing on investigating the charge transfer mechanisms inherent in metal-organic frameworks (MOFs). He is committed to unraveling the complexities of charge transfer within these materials, with the goal of enhancing our fundamental understanding and improving the performances of new materials in this domain.

Amanda Morris* is the Patricia Caldwell Faculty Fellow and Professor of Inorganic and Energy Chemistry at Virginia Tech. Her research education, conducted at Penn State University (B.S.), Johns Hopkins University (Ph.D.), and Princeton University (Postdoctoral), was focused on addressing critical environmental issues with fundamental science including water remediation, solar energy harvesting and storage, and carbon dioxide conversion. As her publication record shows, Morris is a classically trained photo-electrochemist with demonstrated success utilizing various techniques (cyclic voltammetry, spectroelectrochemistry, and pulsed-laser spectroscopy) to explore new frontiers in renewable energy. Her research group's current focus is on light-matter interactions and catalysis. She has received numerous awards for her research pursuits listed below. In addition to her academic pursuits, Morris has a demonstrated record in service including the recruitment and retention of minority chemists. In recognition of this work, she has received the Alan F. Clifford Service Award and College of Science Diversity Award. She currently serves as an American Chemical Society Expert in the area of Sustainable Energy and through this effort has worked to communicate science to the broader national audience with interviews on NPR, newspaper editorials, and press conferences. She also serves as an Associate Editor of Chemical Physics Reviews and sits on the Editorial Advisory Boards for ACS Applied Energy Materials and EnergyChem.

Honors and Awards

Jimmy W. Viers Teaching Award 2022
ACS Pride Chair 2022
GRC Photochemistry Vice-Chair 2021-2023
Patricia Caldwell Faculty Fellow
Kavli Frontiers of Science Fellow
Inter-American Photochemical Society Young Investigator Award
John C. Schug Research Award
Dreyfus Teacher-Scholar Award
Alfred P. Sloan Research Fellow
NSF CAREER Award Recipient
Past Chair of Energy Subdivision, Division of Physical Chemistry, American Chemical Society

Past Chair of Solid-State Subdivision, Division of Inorganic Chemistry, American Chemical Society
Alan F. Clifford Faculty Service Award
American Chemical Society Expert in Sustainable Energy
Diversity Development Institute – Ally Certificate, Advocate Certificate
College of Science Diversity Award
Virginia Tech Scholar of the Week
Ralph E. Powe Junior Faculty Enhancement Award

TOC

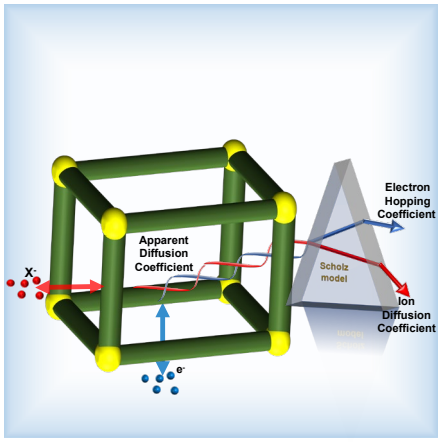
Apparent
Diffusion
Coefficient
X-
e-
Scholz
model
Electron
Hopping
Coefficient
Ion
Diffusion
Coefficient